Synthesis of cRGD peptide cluster-decorated NIR-fluorescent PISA-RAFT nanoparticles targeting integrin expressing cells

Damien Duret, Adrien Grassin, Maxime Henry, Pierre Alcouffe, Sebastian Raja, Carlos Baleizão, José Paulo Farinha, Marie-Thérèse Charreyre, Didier Boturyn, Jean-Luc Coll, et al.

ARTICLE

Synthesis of cRGD peptide cluster-decorated NIR-fluorescent PISA-RAFT nanoparticles targeting integrin expressing cells

Received 00th January 20xx,
Accepted 00th January 20xx

DOI: 10.1039/x0xx00000x

Damien Duret,[a] Adrien Grassin,[b] Maxime Henry,[c] Pierre Alcouffe,[a] Sebastian Raja,[d] Carlos Baleizao,[d] José Paulo Farinha,[d] Marie-Thérèse Charreyre,[a] Didier Boturyn,[b] Jean-Luc Coll,[c] Arnaud Favier *[a]

Surface chemistry has a critical influence on the behavior of nanoparticles in biological media. Moreover, the presence, number, location and organization of surface ligands are important parameters for their selective interaction with cells. In this study, we explored the synthesis of "hairy" polymer nanoparticles presenting a cRGD peptide cluster ligand precisely located at the polymer α-chain-end of the hairs. These polymer nanoparticles were prepared by polymerization-induced self-assembly mediated by the RAFT process (PISA-RAFT) thanks to the synthesis of an original RAFT control agent functionalized with a cRGD tetravalent peptide cluster. Optimization of the PISA-RAFT synthesis led to 50-60 nm spherical hairy nanoparticles that incorporated in their hydrophobic core a crosslinker for stability and near-infrared fluorophores for optical bioimaging. Finally, cRGDcluster-decorated Cy5.5-fluorescent nanoparticles were prepared and both confocal microscopy and flow cytometry demonstrated their ability to selectively recognize cells over-expressing at their membrane integrins that are the natural protein receptor of cRGD ligands.

Introduction

The rise of nanomedicine has motivated the development of an ever-increasing number of organic, inorganic, metallic and hybrid nanoparticles for potential diagnostic, imaging, therapeutic and even theranostic applications.[1] Yet, one of the main challenges is to confer the nanoparticles the ability to selectively interact with biological targets such as protein receptors at the surface of cells. Selective or active recognition is largely related to the surface properties of the nanoparticles and is usually promoted by surface-grafting of biological ligands (*e.g.* saccharides, folic acid, antibodies, peptides, aptamers) able to selectively bind the considered protein receptor. With their high surface area, nanoparticles offer the possibility to immobilize multiple copies of these ligands and thus to improve target recognition through multivalency effects.[2] Generally, the nanoparticles are prepared first, followed by immobilization of the ligands onto their surface using various available chemical groups. However, it remains difficult to control the number, the localization and the organization of the ligands at the surface, although these parameters have a critical impact on the final properties of the nano-objects. For instance, Hammond et al. have prepared "patchy" micelles with folate-clustered ligands at the surface and have shown that the way the ligand is presented on the nanoparticle has a significant influence on cell recognition and internalization.[3]

Since early reports, polymerization-induced self-assembly (PISA), especially via reversible addition-fragmentation chain transfer process (PISA-RAFT),[4-6] has become an established technique for the preparation of various kinds of polymer nanostuctures.[7-10] Their self-assembly is promoted, during polymerization, by the RAFT chain-extension of a solvophilic polymer (MacroCTA) with a solvophobic polymer block. Using this technique in aqueous media, a wide range of nanoparticles can be produced such as spheres, worms and vesicles (polymersomes). These nanoparticles are sometimes referred as "hairy" since their hydrophobic segregated core is stabilized by the soluble hydrophilic polymer chains, avoiding the use of potentially leaking molecular surfactants like in conventional emulsion polymerization. Parameters such as size, shape and physico-chemical properties of the nanoparticle can be tuned by carefully selecting the hydrophilic and hydrophobic polymer blocks. PISA and PISA-RAFT thus have the potential to give access to a large variety of precisely controlled nano-objects for various applications in the biomedical field.

In this study, our objective was to investigate the synthesis of nanoprobes for optical bioimaging based on spherical PISA-RAFT nanoparticles that would exhibit an original combination

[a] *Université de Lyon, CNRS, Université Lyon 1, INSA Lyon, Université Jean Monnet, UMR 5223, Ingénierie des Matériaux Polymères, F-69621 Villeurbanne, France.*
[b] *University Grenoble Alpes, CNRS, UMR 5250, Department of Molecular Chemistry, 38000 Grenoble, France.*
[c] *University Grenoble Alpes, Institute for Advanced Biosciences, Team Cancer Targets and Experimental Therapeutics, INSERM U1209, CNRS UMR5309, Grenoble 38100, France.*
[d] *Centro de Química Estrutural, Institute of Molecular Sciences and Department of Chemical Engineering, Instituto Superior Técnico, University of Lisbon, P-1049-001 Lisbon, Portugal.*

Electronic Supplementary Information (ESI) available: [Complementary experimental data, analyses of the cRGDcluster-CTA, Cy5.5-Am and PDI-BisMAm monomers, PNAM-CTA, cRGD-peptide-cluster and nanoparticles, TEM and cryoTEM images as well as PISA-RAFT kinetics]. See DOI: 10.1039/x0xx00000x

of both i) fluorescence emission in the far-red/near-infrared (NIR) range and ii) surface ligand clusters for bio-targeting. In this spectral range, scattering of light and auto-fluorescence of the biological components are indeed low, thus enabling *in cellulo* and *in vivo* bioimaging with an improved signal-to-noise ratio.[11-13] Concerning the surface ligands, our aim was to elaborate nanoparticles able to recognize cells expressing integrins, that are protein receptors actively involved in important biological processes such as cell adhesion or physiological and tumor angiogenesis.[14-16] The natural ligands of $\alpha_v\beta_3$-integrins, and to a lower extent $\alpha_v\beta_1$-integrins, are RGD peptides (−Arg−Gly−Asp−), a sequence commonly found in extracellular matrix components such as vitronectin and fibronectin. Compared to their linear counterpart, cyclic RGD peptides (cRGD)[17] exhibit an improved affinity for integrins both *in vitro* and *in vivo* and have been clinically evaluated.[18] In addition, a multivalent presentation of cRGDs has led to a further increase in avidity (compared with monovalent cRGD) for integrin-expressing targets and can be advantageously used to develop new drugs and diagnostic agents.[19, 20] Here, we thus selected as ligand a tetravalent cRGD peptide cluster (cRGDcluster, Figure 1) with already proven integrin-recognition capabilities.[20-23]

To synthesize PISA-RAFT nanoparticles with the above-mentioned characteristics, we considered functionalization of both the core and the surface of the nanoparticles. On the one hand, for the fluorescent properties, we studied the introduction of far-red/near-infrared (NIR) polymerizable dyes inside the hydrophobic core of the nanoparticles. One the other hand, to introduce the clustered ligand at the surface of the PISA-RAFT nanoparticles, we explored the biofunctionalization of the hydrophilic block. The ligands could be introduced in lateral position of the hydrophilic chains (for instance via some monomer units)[24]; however, in this case, they might be partially buried inside the polymer corona. Biomolecules can also be themselves used as macroCTA.[10, 25-27] However, in this case, the biomolecule ultimately remains close to the core surface and thus may be not fully accessible or even denatured. Alternatively, we chose to functionalize the α-chain-end of the hydrophilic block that offers a unique opportunity to expose the clustered ligand at the outside periphery of the nanoparticles (Figure 1).[6] The preparation of such α-ligand polymer chains therefore required the prior synthesis of a new original tetravalent peptide-functionalized RAFT chain-transfer agent (cRGDcluster-CTA).

PISA-RAFT synthesis of “hairy” spherical polymer nanoparticles was first optimized without the peptide cluster. These nanoparticles were composed by a poly(*n*-butyl acrylate) (PnBA) core stabilized by hydrophilic poly(*N*-acryloymorpholine) (PNAM) chains at the surface. The introduction in the hydrophobic core of a crosslinker and NIR-fluorescent monomers was also explored. Then, a α-cRGDcluster PNAM hydrophilic block (macroCTA) synthesized from the cRGDcluster-CTA was used to produce PISA-RAFT nanoparticles decorated with the clustered ligand. Finally, the ability of the resulting cRGDcluster-decorated PISA-RAFT nanoparticles to recognize $\alpha_v\beta_3$-integrins was evaluated *in cellulo* by confocal microscopy and flow cytometry, thanks to their NIR fluorescence emission.

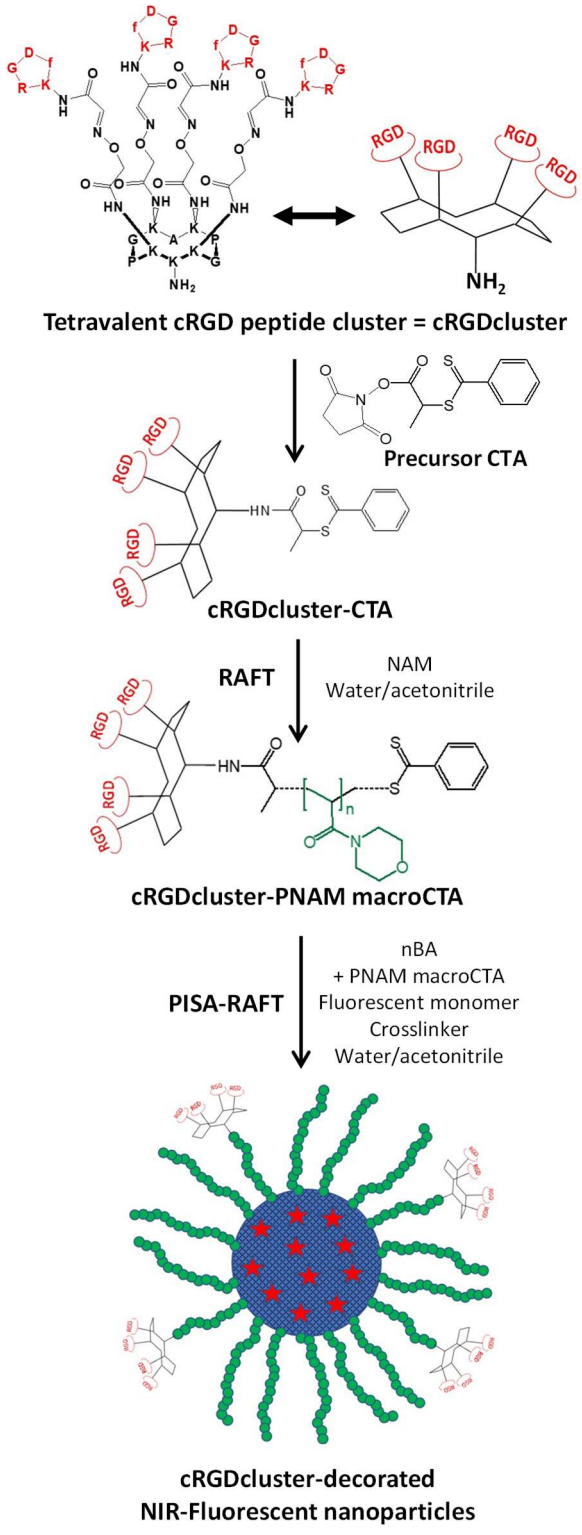

Figure 1. Synthesis of cRGDcluster-decorated NIR-fluorescent PISA-RAFT nanoparticles

Experimental

Materials.

N-acryloyl morpholine (NAM) (Aldrich, 97%) and *n*-butyl acrylate (nBA, Aldrich, ≥99%) were distilled under reduced pressure to remove inhibitor. 1,4-butanediol diacrylate (BDA, Aldrich 90%) was purified on an inhibitor removal column (Aldrich). 2,2'-Azobis(isobutyronitrile) (AIBN, Fluka, ≥98%) was purified by recrystallization from ethanol (Carlo Erba). *N*-acryloxysuccinimide (NAS)[28] and *tert*-butyl dithiobenzoate (tBDB)[29] were synthesized as previously described. 1,4-dioxane (Sigma-Aldrich, ≥99,5%) was distilled over $LiAlH_4$ (Aldrich). Acetonitrile (Fisher, HPLC grade) was distilled in presence of phosphorus pentoxide (Aldrich). *N*,*N*-diisopropylethylamine (DIPEA, Sigma-Aldrich, ≥99,5%), anhydrous *N*,*N*-dimethylformamide (DMF, Acros, 99.8%), trifluoroacetic acid (TFA, Acros, 99%), Cyanine5.5-amine dye (Cy5.5, Lumiprobe), 1,3,5-trioxane (Aldrich, 99%), 4,4'-Azobis(cyanopentanoic acid) (ACPA, Fluka, ≥98%), $NaHCO_3$ (Merck) and diethyl ether (Et_2O, Sigma-Aldrich, ≥99.5%) were used as received.

Peptide-CTA (cRGDcluster-CTA).

Succinimidoxycarbonylethyl dithiobenzoate (7.1 mg, 22.0 µmol), synthesized[30] and purified[31] according previously published procedures, was reacted with the tetravalent cRGD peptide cluster[20] (cRGDcluster, 49 mg, 11.0 µmol) in anhydrous DMF (2.4 mL) in the presence of DIPEA (23.0 µL, 122.2 µmol) for 150 min at 40°C under magnetic stirring. The resulting cRGDcluster-CTA was then purified by reverse phase - ultrahigh pressure liquid chromatography (RP-UHPLC, 1.20 min r.t; C18; 214 nm; 5-100% B over 20 min) (Figure S1 in Electronic Supporting Information, ESI), before freeze-drying (pink powder, 17.4 mg, 4.26 µmol~~, 39% yield~~). Yield was 39% after purification by RP-HPLC due to the unavoidable losses associated with the purification process of such low amount of product. ESI-MS: $C_{181}H_{261}N_{55}O_{51}S_2$; *m/z* $[M + H]^+$; Calculated: 4087.5; found: 4087.1.

Cy5.5-Am fluorescent monomer.

Amino-modified Cy5.5 dye (10 mg, 13.3 µmol) was reacted with *N*-acryloxysuccinimide (2.5 mg, 15.0 µmol) in 750 µL of chloroform at room temperature for 3h under magnetic stirring. The Cy5.5-Am product was precipitated in diethyl ether before purification by silica gel chromatography with a chloroform/methanol 80/20 vol/vol eluent (blue powder, 5.7 mg, 56% yield).

RMN ^1H (300.13 MHz, $CDCl_3$) (Figure S2): 8.08 (m, 2H), 8 (m, 1H), 7.93 (m, 4H), 7.76 (m, 1H), 7.60 (m, 2H), 7.46 (m, 2H), 7.35 (m,2H), 7.04 (t, 1H), 6.65 (d, 1H), 6.55 (dd, 1H), 6.27 (t, 1H), 6.23 (d, 1H), 4.49 (dd, 1H), 4.21 (t, 2H), 3.70 (s, 3H), 3.34 (q, 2H), 3.25 (q, 2H), 2.42 (t, 2H), 1.99 (d, 9H), 1.91 (m, 2H), 1.81 (m, 2H), 1.6 (m, 10 H), 1.41 (s, 3H).

PDI-BisMAm NIR-fluorescent crosslinker.

The synthesis of the PDI-BisMAm NIR-fluorescent crosslinker followed Scheme S1 and is detailed in ESI.

RAFT solution polymerizations.

Synthesis of PNAM macroCTA. RAFT polymerization was adapted from a previously optimized procedure.[32] Briefly, NAM (10 g, 70.8 mmol), tBDB (178.4 mg, 0.85 mmol), AIBN (13.9 mg, 84.8 µmol) and trioxane (531.7 mg, used as reference for ^1H NMR determination of monomer conversion) were dissolved in 26.5 mL of dioxane and placed in a Schlenk tube. The solution was degassed by 5 freeze-pump-thaw cycles and heated at 80°C under nitrogen (81% conversion). PNAM macroCTA was purified by two consecutive precipitations in diethyl ether and dried under vacuum up to constant weight.

Synthesis of cRGDcluster-PNAM macroCTA. NAM (91.5 mg, 648.2 µmol), cRGDcluster-CTA (17.4 mg, 3.83 µmol), 64.4 µL of an aqueous solution of ACPA (24µmol L^{-1}) with $NaHCO_3$ (83 µmol L^{-1}), and trioxane (3.24 mg, used as reference for ^1H NMR determination of monomer conversion) were dissolved in 500 µL of a water/distilled acetonitrile/TFA 49.5/49.5/1 vol/vol/vol mixture. The solution placed in a Schlenk tube was de-oxygenated by three freeze-pump-thaw cycles, before stirring and heating at 80°C under nitrogen (18% conversion). After evaporation of the solvents, the polymer was solubilized in a chloroform/DMF mixture, purified by two consecutive precipitations in diethyl ether and dried under vacuum up to constant weight.

PISA-RAFT synthesis of nanoparticles (Table S1).

Typically, PNAM macroCTA (202 mg, 17.9 µmol), 301 µL of an aqueous solution of ACPA (24µmol L^{-1}) with $NaHCO_3$ (83 µmol L^{-1}), and trioxane (21.1 mg, used as reference for ^1H NMR determination of nBA conversion) were mixed in 2.4 mL of solvent (water or water/distilled acetonitrile 50/50 vol/vol) in a 20 mL Schlenk tube. 403 µL of distilled nBA were then added. The biphasic solution was de-oxygenated by 4 freeze-pump-thaw cycles, vigorously stirred and heated under nitrogen at 80°C. Samples were regularly withdrawn from the reaction medium to follow polymerization kinetics (by ^1H NMR) and the evolution of the average particle size with conversion (by QELS). After polymerization, nanoparticle dispersions were diluted with mQ water before purification by dialysis (SpectraPor6, MWCO 50 kDa MWCO) and gentle filtration over a 0.45 µm pore-size membrane.

Fluorescent and crosslinked PISA-RAFT nanoparticles. The same above-mentioned protocol was followed except that the indicated amount of fluorescent monomer (Cy5.5-Am or PDI-BisMAm) and BDA crosslinker were introduced with the distilled nBA solution at the indicated proportions (Table S1).

cRGDcluster-decorated nanoparticles. The previous protocol was adapted as follows: cRGDcluster-PNAM-DB (1.9 mg, 0.19 µmol), tBu-PNAM-DB (82.6 mg, 7.31 µmol), 126 µL of an aqueous solution of ACPA (24µmol L^{-1}) with $NaHCO_3$ (83 µmol L^{-1}), and trioxane (8.8 mg) were mixed in a total volume of 1 mL water/distilled acetonitrile (50/50 vol/vol) in a 20 mL Schlenk tube. Distilled nBA (169 µL, 1.18 mmol), BDA (6.3 µL, 33.6 µmol) and Cy5.5-Am (1.4 mg, 1.77 µmol) were then added. The

biphasic solution was de-oxygenated by 4 freeze-pump-thaw cycles, vigorously stirred and heated under nitrogen at 80°C.

Analytical techniques.

Reverse-phase high pressure liquid chromatography (RP-HPLC). RP-UHPLC analyses were performed on Waters equipment consisting of a Waters Acquity H-Class Bio UPLC combined to a Waters SQ Detector 2 mass spectrometer. The analytical column (ACQUITY UPLC BEH C18 Column, 130 Å, 1.7 µm, 2.1 mm x 50 mm) was operated at 0.6 mL.min^{-1} with linear gradient programs in 2.20 min run time (routine program: 5% to 100% B in 2.20 min). UV monitoring was performed at 214 nm. Solvent A consisted of H_2O containing 0.1% formic acid (FA) and solvent B consisted of CH_3CN containing 0.1% FA. Water was of Milli-Q quality. CH_3CN and FA were LC-MS grade.

RP-HPLC purifications were performed on Gilson GX-281. The preparative column (Macherey-Nagel 100 Å, 7 µm C18 particles, 250 x 21 mm) was operated at 20.84 mL.min^{-1}. Linear gradient programs in 30 min run time were used and solvents A and B were the same as the ones used in RP-UHPLC analysis.

Electron spray ionization mass spectrometry (ESI-MS). ESI-MS mass spectra were obtained on an Esquire 3000 (Bruker). The multiply charged data produced by the mass spectrometer on the m/z scale were converted to the molecular weight.

Quasi-elastic light scattering (QELS). Size of the nanoparticles were analyzed at 25°C using a Zetasizer Nano S90 apparatus (Malvern) equipped with a 633 nm 4 mW He-Ne laser. Measurements were performed at 173° angle on highly diluted aqueous solutions that were previously filtered over a 0.45 µm membrane and then placed in 1 cm large glass cuvettes. Average hydrodynamic diameter (D_h) and polydispersity index (PDI) of the nanoparticle samples were determined thanks to the Nano DTS software from a series of 5 repeats of 10 measurements.

Transmission Electron Microscopy (TEM). Observations were performed on a Philips CM 120 electron microscope operating at an accelerating voltage of 80 kV. A drop of aqueous solution of nanoparticles was placed on a carbon coated copper grid (EMS, CFU-200-CU, 200 mesh) and the excess liquid was removed before air-drying of the sample. Polymer nanoparticles were revealed by positive staining using ruthenium oxide (RuO_4): the dried grids were exposed to RuO_4 vapors for 15-20 min. Particle size distribution was then determined using ImageJ software by statistical analysis of 100–300 nanoparticles taken from different images for each sample.

CryoTEM. Samples were prepared by depositing 5 µL of a nanoparticule aqueous dispersion onto a copper grid coated with an advanced holey carbon film (Quantifoil, EMS). The excess of sample was removed by quick blotting using filter paper leaving a thin spanned film on the grid. The latter was immediately vitrified by plunging into liquid ethane cooled by liquid nitrogen (Cryoplunge, Orsay University, Laboratory Physique des solides). The sample was transferred in liquid nitrogen, inserted into a cold cryo-holder (Gatan), and quickly transferred into the vacuum column of the TEM microscope (Philips CM 120) prepared in cryo mode. The accelerating voltage used for the observation was 120 kV.

^{1}H NMR. Spectra were acquired at 300 K on a Bruker Ultrashield spectrometer operating at 300.13 MHz. Polymer macroCTAs were characterized after purification. The dried sample was solubilized in the selected NMR solvent (all from Sigma-Aldrich), $CDCl_3$ for the PNAM macroCTA and D_2O for the cRGDcluster-PNAM macroCTA, before analysis. The NAM average degree of polymerization $DP_{n\ NAM}$ and thus the number-average molecular weight M_n of the chains (Eq. 1) was determined after integration of the spectra by comparing polymer peaks to chain-end peaks coming from the CTA. For the PNAM macroCTA (Figure S3), the polymer morpholine protons (3-4.2 ppm) were compared to the tert-butyl α-chain-end protons (0.8-1 ppm) as previously reported.[32] For the cRGDcluster-PNAM macroCTA (Table S2), 7-8.5 ppm area representing a total of 29 protons coming from the cRGDcluster-CTA was compared to various areas inside the 1-5.2 ppm region where PNAM and peptide peaks are superimposing. The results were very consistent whatever the case scenario and $DP_{n\ NAM}$ was determined to be 44±2 (Table S2).

$$Mn = DPn_{NAM} \times M_{NAM} + M_{CTA} \qquad (1)$$

Monomer conversion for PISA-RAFT experiments was determined from raw samples diluted in deuterated chloroform, $CDCl_3$ (Figure S4). Disappearance of nBA vinylic protons (5.6-6.6 ppm) was followed over time in comparison to the trioxane singlet (5.2 ppm) used as internal reference.[33]

^{1}H DOSY NMR. Diffusion experiments were performed in D_2O/CD_3CN 70/30 v/v using a LED sequence with bipolar pulses (BPPLED). 64 scans were acquired with 16k data points. Gradient intensity was linearly incremented from 1 to 45.7 G cm^{-1} in 30 points. Gradient pulse length was $\delta/2$ = 3.8 ms and diffusion time was Δ = 200 ms. The DOSY spectra were obtained by applying an Inverse Laplace Transform (ILT) along the diffusion axis using the commercial NMR Notebook software (NMRTEC, Illkirch, France).

SEC/MALLS. Size exclusion chromatography coupled with multi-angle laser light scattering detection (SEC/MALLS) was performed using a set up composed of a Shimadzu LC-6A liquid chromatography pump and a PLgel Mixed-C column (5 mm pore size). Online double detection was provided by a differential refractometer (DRI Waters 410) and a three-angle (46, 90 and 133°) MiniDAWN TREOS light scattering photometer (Wyatt Technologies), operating at 658 nm. Analyses were performed by injection of 70 µL of polymer solution (5 mg.mL^{-1}) in chloroform.

The specific refractive index increment (dn/dc) for PNAM homopolymer in the same eluent (0.130 mL.g^{-1}) was previously determined with a NFT ScanRef monocolor interferometer operating at 633 nm. The molar mass and polydispersity data were determined using the Wyatt ASTRA SEC/LS software package.

Biological evaluation.

Cell culture. Cell lines were maintained at 37°C in a humidified 95% air/5% CO_2 incubator. HEK293(β3) and HEK293(β1) cells are stable transfectants of the human embryonic kidney cell line overexpressing the integrin ß3 or ß1 respectively (kindly provided by J.-F. Gourvest, Aventis, France). The HEK293-derived cells were cultured in DMEM plus 10% FBS supplemented with 700 $\mu g.mL^{-1}$ Geneticin (G418 sulfate; Gibco, Paisley, UK).

Confocal Microscopy. The wells of Labtek glass coverslips (NUNC) were coated with a $5\mu g.mL^{-1}$ solution of vitronectin in phosphate buffer (PBS) for 1 h at room temperature and then saturated with a 3% PBS solution of bovine serum albumin (BSA) for 30 min at room temperature. Wells were rinsed with PBS. 10 000 cells per well were plated in DMEM with 10% fetal calf serum (FCS) for 24 h. After 2 washes with PBS, the tested compounds were added at the desired concentration in DMEM with 10% FCS before incubation for 30 min at 37°C. After two PBS washes, cells were fixed with a 0.5% p-formaldehyde (PFA) solution and their nuclei were stained using a 5µM Hoechst solution for 15 min. After two PBS washes, cells were maintained in PBS and then observed by confocal microscopy on a Zeiss LSM710 NLO – LIVE7 – Confocor3 microscope. Excitation wavelengths λ_{ex} were respectively 405 and 633 nm for Hoechst and Cy5.5 dyes.

Flow cytometry. HEKβ3 cells were re-suspended with trypsin then rinsed once with PBS and twice with PBS containing 1 mM $CaCl_2$ and 1 mM $MgCl_2$. 1 million cells in a 200 µL final volume were incubated for 20 min at 37°C with the tested compounds at the desired concentration in PBS with 1 mM $CaCl_2$ and 1 mM $MgCl_2$. Compound solution was removed and the cells rinsed 2 times with the same buffer. Finally, cells were rapidly analyzed by flow cytometry (λ_{ex} = 640 nm) on an Accuri C6 (Becton Dickinson) apparatus and the CFlow Plus software.

Results and discussion

As explained in the introduction, PISA-RAFT nanoparticles can be viewed as "hairy" as they are sterically stabilized by the soluble polymer blocks at their surface (Figure 1). Therefore, in aqueous media, their surface properties can be tuned according to the kind of hydrophilic polymer selected as the RAFT macromolecular chain transfer agent (macroCTA). Moreover, the α-chain-end of this macroCTA will be located at the extremity of the hairs, thus preferentially at the periphery of the PISA-RAFT nanoparticles. For this study, we synthesized two different RAFT macroCTAs (Table 1), both based on poly(*N*-acryloylmorpholine) (PNAM) chains. PNAM is indeed a neutral hydrophilic and biocompatible polymer that exhibits similar properties than poly(ethyleneglycol), PEG, known to limit nonspecific bio-interactions.[34] The first PNAM macroCTA was prepared with an inert α-chain-end using the already described tert-butyl dithiobenzoate RAFT CTA, whereas the second cRGDcluster-PNAM macroCTA was synthesized from a new original CTA carrying the tetravalent cRGD peptide cluster (cRGDcluster-CTA).

Synthesis of a RAFT chain transfer agent (CTA) functionalized by a tetravalent cRGD peptide cluster.

The considered cluster (cRGDcluster, Figure 1), prepared based on previously reported methods,[35] is based on a cyclodecapeptide platform that displays in a spatially controlled manner, (i) an integrin recognition domain presenting 4 cRGD ligands and, on the opposite side, (ii) a lysine primary amine for the regioselective conjugation with different moieties.[20, 36, 37] Thanks to the constrained multivalency, $\alpha_v\beta_3$ integrin binding is improved compared to the monovalent cRGD.[20, 35, 38, 39] Integrin recognition is specific as demonstrated using a cRβAD-cluster negative control.[20] In addition, the benefit of the tetravalent cluster compared to the monovalent ligand was confirmed on grafted surfaces.[40] We have also reported the successful regioselective conjugation of multiple copies of this peptide cluster onto a poly(*N*-acryloylmorpholine-*stat*-*N*-acryloxysuccinimide), P(NAM-*stat*-NAS) copolymer chains, leading to "polymultivalent" polymer ligands that exhibit remarkable targeting properties for cells over-express integrins.[21]

To synthesize the RAFT CTA functionalized with the tetravalent cRGD peptide cluster (cRGDcluster-CTA, Figure 1), the lysine primary amine group of the peptide cluster was reacted in DMF at low temperature (40°C) with the activated ester group of a precursor CTA that was developed in our lab.[30] A highly pure compound (39% overall yield after purification) was obtained by preparative RP-HPLC (Figure S1), after optimization of the elution profile (see experimental part). Finally, ESI-MS analysis confirmed the successful synthesis of the cRGDcluster-CTA, the main peaks corresponding to the 4^+, 3^+ and 5^+ adducts (Figure 2).

Synthesis of PNAM-based macroCTAs by RAFT polymerization.

Two types of PNAM-based polymer chains were synthesized by RAFT polymerization with a molecular weight close to 10 000 $g.mol^{-1}$ to later serve as hydrophilic macroCTAs for the elaboration of the PISA-RAFT nanoparticles. These macroCTAs differed by their α-chain-end, thus by the CTA that was used to perform the RAFT polymerization. The first one, without peptide cluster, was synthesized with tert-butyl dithiobenzoate (tBDB) as the CTA to obtain PNAM chains with an inert α-chain-end (PNAM macroCTA), whereas the second was synthesized in the presence of the cRGDcluster-CTA in order to prepare PNAM chains functionalized at their α-chain-end by the cRGD peptide cluster (cRGDcluster-PNAM macroCTA) (Table 1).

Table 1. PNAM macroCTAs synthesized by RAFT polymerization

MacroCTA	Monomer	α-chain-end	$M_{n\ NMR}$ g.mol^{-1}	DP_{NAM}
PNAM	NAM	tBu	11 300	79
cRGDcluster-PNAM	NAM	Tetravalent peptide cluster	10 300	44

DP_{NAM} and $M_{n\ NMR}$ are respectively the average number of NAM units (degree of polymerization) per macroCTA and the number-average molecular weight, including the chain-ends, both determined by ^{1}H NMR after polymer purification, as detailed in the experimental part.[32]

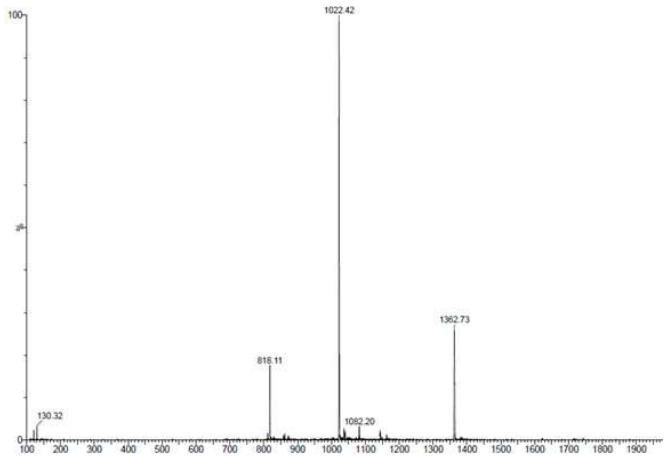

Figure 2. ESI$^+$-MS spectrogram of the purified cRGDcluster-CTA ($C_{181}H_{261}N_{55}O_{51}S_2$). m/z: $[M+5H]^{5+}$ found 818.11, calculated 818.49; $[M+4H]^{4+}$ found 1022.42, calculated 1022.87; $[M+3H]^{3+}$ found 1362.73, calculated 1363.49.

We have previously optimized the RAFT homo- and co-polymerization of NAM in the presence of various dithiobenzoate CTAs, such as tBDB.[29] In rather short polymerization times (<2 hours), polymer chains with a controlled molecular weight and chain-end functionality have been obtained with a low dispersity.[32] This optimized protocol was used here to prepare the PNAM macroCTA sample (M_n = 11 300 g.mol^{-1}) in dioxane (Figure S3).

Nonetheless, it was not obvious that applying these optimized conditions would lead to a successful RAFT polymerization of NAM in the presence of the bulkier cRGDcluster-CTA. In addition, solvent was changed to a water/acetonitrile/TFA mixture 49.5/49.5/1 (vol%) that appeared to be a good solvent of the cRGDcluster-CTA, monomer and growing polymer chains. The resulting polymer sample purified by precipitation in diethyl ether was then characterized by both ^{1}H NMR and ^{1}H DOSY NMR in D_2O/acetonitrile-d 70/30 vol%. ^{1}H DOSY NMR spectrum (Figure 3A) exhibited only one diffusion line gathering the ^{1}H NMR signals from both the cRGD peptide cluster (Figure S5) and PNAM chain (Figure S3). It thus demonstrated the presence of the tetravalent peptide cluster at the PNAM α-chain-end after RAFT polymerization. Furthermore, the ^{1}H NMR spectrum (Figure 3B) exhibited the characteristic aromatic proton signals corresponding to the dithiobenzoate ω-chain-end. Integration of this spectrum enabled the determination of the NAM average degree of polymerization ($DP_{n\ NAM}$ = 44), and thus the calculation of a M_n value of 10 300 g.mol^{-1} for the cRGDcluster-PNAM macroCTA (see experimental part).

ARTICLE

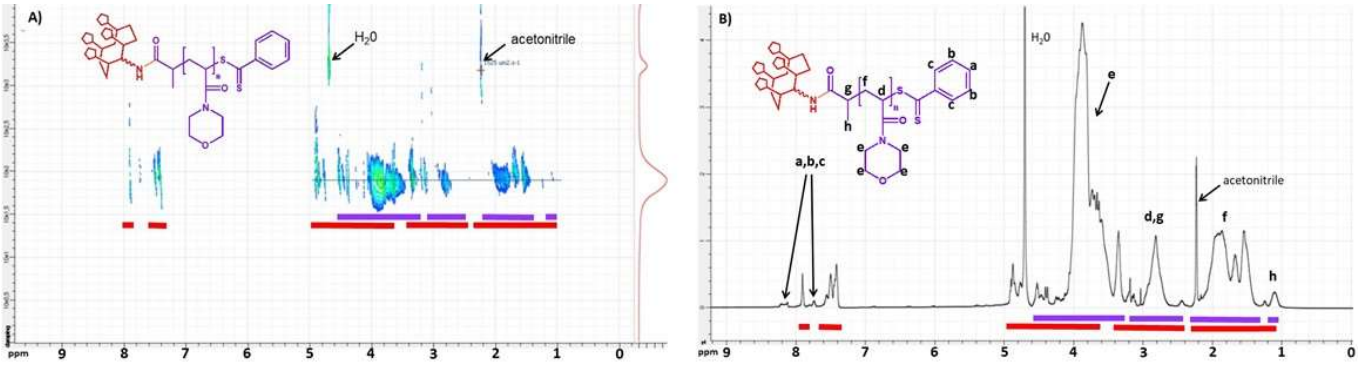

Figure 3. ^{1}H DOSY NMR (A) and ^{1}H NMR (B) spectra of the purified cRGDcluster-PNAM macroCTA in D_2O/acetonitrile-d 70/30 vol%. For clarity, red and **purple** lines indicated the regions associated with peaks of the peptide cluster and the polymer, respectively (see Table S2 for details).

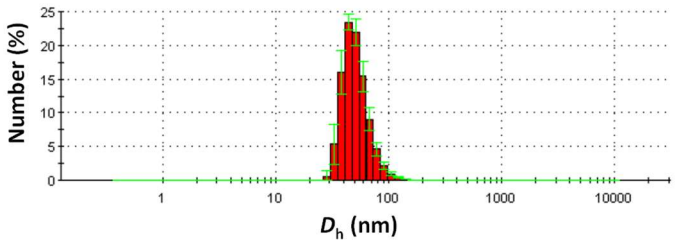

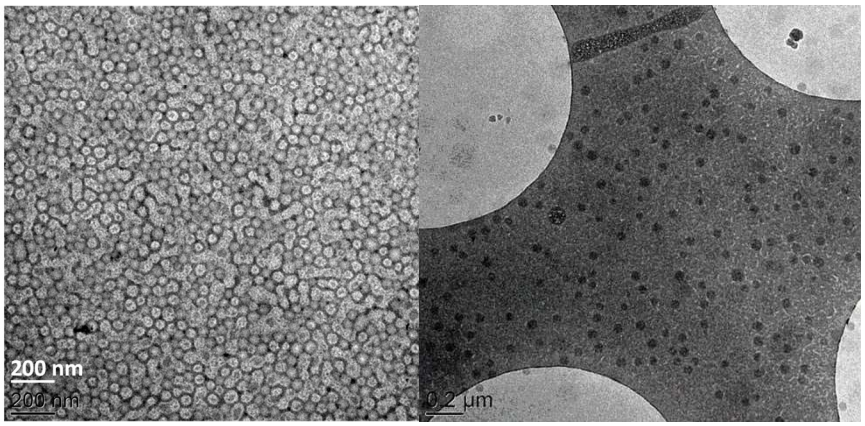

Figure 4. (Top) Distribution of D_h values measured by QELS for the reference experiment **5** in Table S1 (monomer conversion = 83%, average D_h = 51 ±17nm). Corresponding intensity distribution is given in ESI, Fig. S8. (Bottom) Corresponding TEM (left) and cryoTEM (right) images (scale bar 200 nm). On the cryoTEM images (bottom right), the nanoparticles were mainly located on top of the carbon support (dark grey area) and few of them on the edge of the holes (light grey areas). Dark crystals corresponded to ice crystals formed during the cryo process.

Optimization of nanoparticle synthesis by PISA-RAFT with the PNAM macroCTA.

Overall, PISA-RAFT experiments were performed in aqueous media using *n*-butyl acrylate (nBA), as a model hydrophobic monomer that enables a good blocking efficiency with the acrylamide-based macroCTAs.[41] Azobiscyanopentanoic acid (ACPA) was chosen as a water-soluble initiator. In a first step, before using the cRGDcluster-PNAM macroCTA, a thorough optimization was conducted with the PNAM macroCTA (M_n = 11 300 g.mol^{-1}). In order to prepare spherical PISA-RAFT nanoparticles, the influence of several key parameters was studied both on polymerization kinetics and size of the resulting nanoparticles.

The initiator concentration was first varied to obtain high nBA conversion (>80%) in a rather short time (<6h) in order to avoid potential degradation of the fluorophores/peptides later in the study. The aqueous continuous phase solubilizing the macroCTA

and the initiator was deionized water for these first experiments and the initial nBA concentration was 1M. The initial nBA/macroCTA molar ratio was set at 156.3 (representing a 2/1 weight ratio between the hydrophobic and hydrophilic blocks at full nBA conversion) to favor the formation of spherical nanoparticles. Increase of the initiator concentration should lead to faster kinetics but may also cause a loss of control over the PISA-RAFT process.[41] Thus, comparable assays were performed at different macroCTA/initiator molar ratios of 2, 2.5, 3 and 5 (Exp. **1**-**4** in Table S1). As expected, polymerization rate increased when increasing the initiator concentration (thus decreasing the macroCTA/initiator ratio). Full nBA conversion was obtained in 2h for ratio = 2, whereas almost no nBA conversion was observed for ratio = 5 (Figure S6). Moreover, when occurring, polymerization successfully led to the formation of spherical nanoparticles with a poly(*n*-butyl acrylate) core (PnBA) stabilized by PNAM hydrophilic chains. For the rest of the study, the 2.5 ratio was selected. In this case, >90% nBA conversion was reached after 5h and the nanoparticle average size was ≈ 50-60 nm, as determined by QELS measurements (Figure 4, Top)

Then, water was replaced by a mixture of water/distilled acetonitrile 50 vol% as the continuous solvent phase, since it was necessary for the PISA-RAFT experiments with the cRGDcluster-PNAM macroCTA (see below). In this solvent mixture, polymerization kinetics and nanoparticle size were globally similar compared with pure water (Figure S7). Several assays reproducibly led to 80-90% conversion after 5 hours polymerization and to 50-65 nm average nanoparticle size.

During one experiment (Exp. **5** in Table S1), samples were regularly withdrawn from the reaction medium during the PISA-RAFT process to follow polymerization kinetics (Figure S7), and the evolution of the average particle size with conversion (Figure S8). At the beginning of the polymerization, monomer conversion increased slowly (induction period) as the process is mainly taking place in the aqueous phase where nBA concentration is low. However, once the amphiphilic poly(NAM-*block*-nBA) copolymers started to self-assemble into micelles, swelled by nBA, monomer conversion increased rapidly. The micellar solution was then highly stable (no demixing when stirring is stopped). Interestingly, the partition of acetonitrile between the aqueous and the organic phase had a little influence on the self-assembly process. The presence of acetonitrile tended to shorten the induction period and to slightly decrease the polymerization rate after self-assembly. This may be attributed to the fact that the partition of acetonitrile favors an increase of the nBA concentration in the continuous phase and a dilution of nBA inside the swollen core of the self-assembled nanoparticles.

Concerning the evolution of the nanoparticle size with conversion, at 58% conversion (2.5 h), the average size of the nanoparticles was around 40 nm and reached more than 50 nm after 80% conversion (5h), in accordance with the increase of the PnBA core size (Figure S8). The size of the latter nanoparticle sample was then further confirmed by TEM and cryoTEM (Figure 4, bottom). By TEM, core-shell nanoparticles were clearly observed after RuO_4 staining of the PNAM corona (Figure 4, bottom left and Figure S9).[42] Observations were nonetheless impaired by the tendency of the nanoparticles dried on the TEM grid to rapidly fuse when exposed to the electron beam, because of the low T_g of PnBA (Figure S10). A cryoTEM analysis was then conducted to image the nanoparticles trapped inside a frozen water film (Figure 4, bottom right and Figure S11). For the same sample (QELS D_h = 51 ±17 nm), the average diameter was 53 ±8 nm for the core-corona nanoparticles (cryoTEM) and 38 ±7 nm for the core only (TEM). Thus, electron microscopy results were in close agreement with QELS, further confirming the size of the nanoparticles (Table S3). Moreover, even if no systematic study was performed, nanoparticle dispersions were very stable as observed for several samples that could be stored for at least 6 months without change in their measured diameter (by QELS).

This reproducible experimental protocol was then used as a basis to investigate the influence of the addition of a crosslinker and a fluorescent monomer inside the hydrophobic core of the nanoparticles.

Synthesis of NIR-fluorescent core-crosslinked PISA-RAFT nanoparticles.

Influence of the addition of a hydrophobic crosslinker. To further stabilize the PnBA core of the nanoparticles, a crosslinker can be added to the hydrophobic phase like in conventional emulsion polymerization.[43] Butanediol diacrylate (BDA) was then chosen as crosslinker due to its structural similarity with nBA. Its concentration was progressively increased from 0 (previously described experiment) to 12 mol% compared to nBA (Exp. **5** to **10** in Table S1). No effect on polymerization and on nanoparticle size was observed up to 9 mol% (Figure S12), except for the highest concentration (12 mol%) for which a macroscopic gel formed during polymerization. For the rest of the study, an intermediate value of 3 mol% of BDA was then arbitrarily chosen.

Influence of the addition of a hydrophobic fluorescent monomer. To fluorescently label the nanoparticles, fluorophores can be either encapsulated or copolymerized as a monomer within the core.[44] The use of hydrophobic fluorescent monomers was preferred here as encapsulation may result in fluorophore leaking.[45] Two types of fluorescent monomers (Figure 5) were synthesized and added to the nBA/BDA mixture at 0.15 mol% (Table S1). The first type was a fluorescent crosslinker based on a perylene diamine dye[46] that emit**s** in the near-infrared ($\lambda_{em\ max}$ = 750 nm), a wavelength range where light penetration depth into the biological tissues is increased. This fluorescent crosslinker has been functionalized to present a methacrylamide group at each opposite side of the perylene molecule (Scheme S1). The second type of fluorophore was a hydrophobic cyanine 5.5-based fluorescent monomer (Cy5.5-Am) that emits in the far-red / near infrared ($\lambda_{em\ max}$ = 700 nm) and that can be conveniently excited by the 633nm laser line of fluorescence microscopes and flow cytometers. This fluorescent Cy5.5-Am monomer was synthesized by coupling of

a corresponding Cy5.5 amino-derivative with NAS and purification was performed by column chromatography (see experimental part, Figure S2).

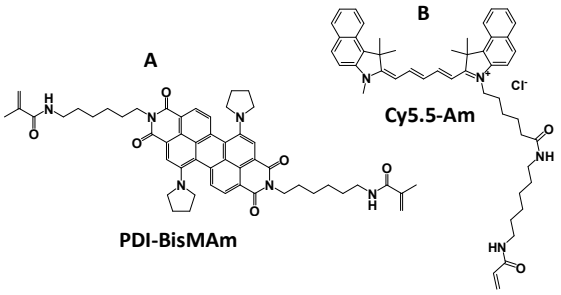

Figure 5. Fluorescent crosslinker (PDI-BisMAm) and monomer (Cy5.5-Am) used this study

Addition of these hydrophobic fluorescent monomers did not affect polymerization and particle size. After dilution and dialysis, the colored nanoparticle samples (green with PDI-BisMAm crosslinker and blue with Cy5.5-Am) were also characterized by UV-Vis and fluorescence spectroscopy (Figure S13-S14). The nanoparticles retained the spectral properties of the corresponding incorporated fluorophores. Based on the nanoparticle overall and core diameters previously determined by QELS and TEM (see above), it has been estimated that such nanoparticle contains an average of 265 fluorophores (Table S4). The fluorescent nanoparticles were thus highly bright, which facilitate their detection by optical microscopy. Interestingly, the nanoparticles dispersed in water presented absorption and fluorescence emission spectra that better resembled the ones of the free dyes in dioxane rather than in water (Figure S14). Indeed, due to solvatochromism, emission of such dyes is usually red-shifted in water compared to less polar solvents. Consequently, these observations demonstrated that the dyes were indeed imbedded and dispersed inside the PnBA hydrophobic core whose polarity is closer to the one of dioxane.

All those results thus demonstrated that the hydrophobic core of the nanoparticles can be further stabilized by the addition of a crosslinker (up to about 10 mol% of BDA) and readily labeled by the copolymerization of different types of hydrophobic fluorescent monomers, without incidence on polymerization kinetics and on final particle size. For the rest of the study, only the core-crosslinked nanoparticles labeled with Cy5.5-Am were selected as their fluorescence properties were more adapted to the detection sensitivity of our confocal microscopy and flow cytometry apparatus.

Synthesis and *in cellulo* evaluation of peptide-decorated NIR-fluorescent PISA-RAFT nanoparticles.

After optimization with the PNAM macroCTA, stable Cy5.5-fluorescent nanoparticles were synthetized in the presence of the cRGDcluster-PNAM macroCTA, the previous PNAM/nBA/BDA/CyAm sample without peptide cluster (**NP1**) serving as reference for comparison (Table 2).

Table 2. Cy5.5-fluorescent PISA-RAFT nanoparticle samples produced from the two different macroCTAs in water/acetonitrile 50/50 vol% as solvent

NP sample	MacroCTA	Cross-linker	Fluorescent Monomer	Conv (%)	$D_{h\ QELS}$ (PDI)
NP1	PNAM	BDA	Cy5.5-Am	85	47 nm (0.15)
NP2	PNAM and cRGDcluster-PNAM (2.5 mol%)	BDA	0	83	52 nm (0.12)
NP3	PNAM and cRGDcluster-PNAM (2.5 mol%)	BDA	Cy5.5-Am	58	63 nm (0.18)

It is noteworthy that surface density of peptide clusters has been shown to be important for the recognition of integrin-presenting targets.[47] Accordingly, having a cRGD cluster (2-3 nm in size)[21] at the end of each "hair" of the nanoparticle would be detrimental for the biotargeting properties. Therefore, to space the clustered ligand at the surface of the nanoparticles, the cRGDcluster-PNAM macroCTA (M_n = 10 300 g.mol^{-1}) was mixed at 2.5 mol% with the PNAM macroCTA without peptide (M_n = 11 300 g.mol^{-1}). Indeed, considering the typical nanoparticle size obtained previously (see above), we estimated that the average number of cRGD-peptide-clusters per nanoparticle would be around 28, corresponding to an average distance between two cRGDclusters close to 18 nm at the periphery of the nanoparticles (Table S4).

PISA-RAFT synthesis was conducted in 50 vol% water/acetonitrile to ensure the full solubility of the cRGDcluster-PNAM macroCTA and two experiments were performed in the presence and in the absence of the Cy5.5-Am fluorescent monomer (**NP2** and **NP3** in Table 2, respectively). In each case, 50-60 nm nanoparticles were obtained and the presence of the cRGDcluster-PNAM macroCTA had no significant influence on polymerization. In addition, thanks to their NIR fluorescence, **NP1** and **NP3** nanoparticles were detectable both by fluorescence microscopy and by flow cytometry to study their ability to recognize integrin-expressing cells. Indeed, the functionalization of the nanoparticles with the cRGD peptide cluster (**NP3**) should favor their interaction with this type of cells in comparison with the nanoparticles that are not functionalized with the peptide cluster (**NP1**).

Confocal fluorescence microscopy and flow cytometry were then used to compare cell internalization of these two types of Cy5.5-fluorescent nanoparticles. They were incubated in the presence of fetal calf serum (FCS) with either HEKβ3 or HEKβ1 cells that are respectively over-expressing the β_3 or β_1 chain of integrins (HEK cells are naturally expressing the α_v chain of integrin). cRGD peptides having more affinity for $\alpha_v\beta_3$-integrins, it was thus expected that the labeling of HEKβ3 cells by the cRGDcluster-decorated nanoparticles would be more pronounced than the labeling of HEKβ1 cells.

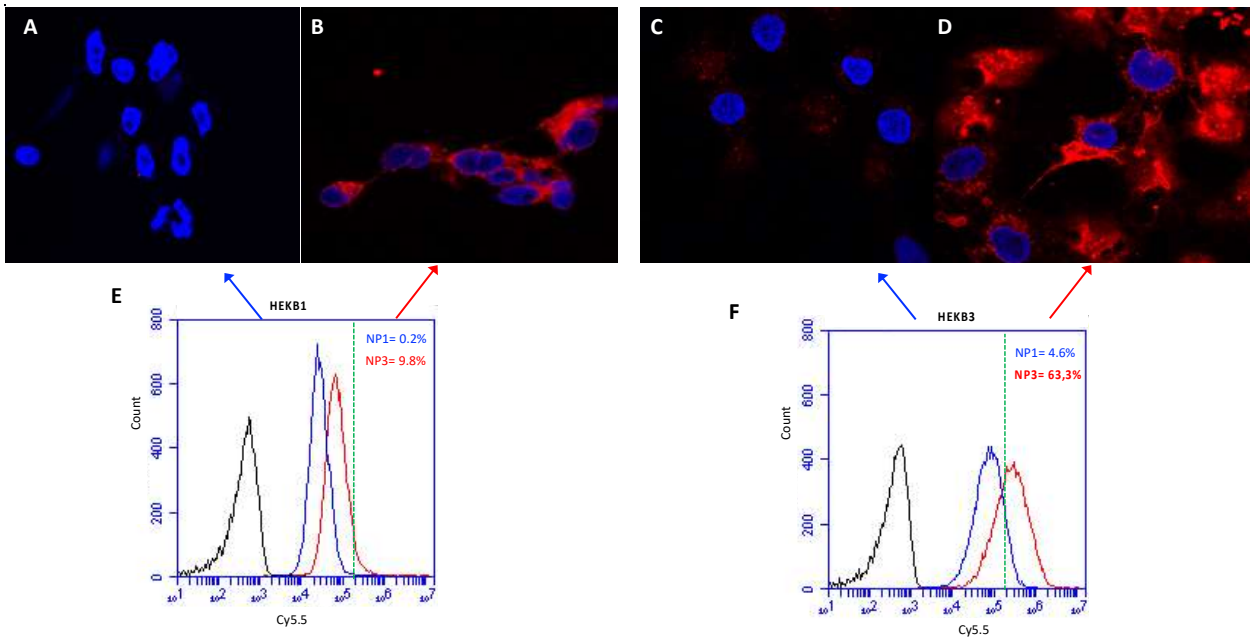

Figure 6. *In vitro* cell labeling of the Cy5.5-fluorescent PISA-RAFT nanoparticles without peptide (**NP1**) or decorated with the tetravalent cRGD-peptide-cluster (**NP3**). NPs (0.1 mg.mL^{-1}) were incubated for 30 min at 37°C with HEKβ3 or HEKβ1 cells in the presence of 10% FCS and observed by confocal microscopy (top panels, A, B, C, D). In blue: Nuclear DNA stained by Hoechst 33342. In red, Cy5.5 labeling. As can be seen on these images, **NP1** are not staining Hekß1 as well as HEKß3 cell lines (A and C respectively) while, in contrast, **NP3** labeling in the cytoplasm of the cells was stronger on HEKß3 cells (D) than HEKß1 (B), indicating the capacity of **NP3** to be internalized within a few minutes. These cells were also analyzed by flow cytometry (E and F). Labeling % values indicated on the graphs (based on the artificial green dashed line cutoff) showed that **NP3** (red curves) more efficiently labeled HEKß3 (63.3%) rather than HEKß1 (9,8%) cells, while **NP1** (blue curves) induced a very low labeling (4.6 and 0.2% respectively). In black, HEKß1 or HEK ß3 cells without any staining (negative control showing the autofluorescence of the cells).

This was indeed confirmed by both flow cytometry and confocal microscopy (Figure 6). Flow cytometry indicated that cell labeling with **NP3** was very efficient with the $\alpha_v\beta_3$-positive HEKß3 cells (63.3%), while it was much lower with **NP1** (4.6%). When the $\alpha_v\beta_3$ integrin is not expressed (HEKß1 cells), cell labeling was low with both **NP1** and **NP3** (0.2 and 9.8% respectively). These results were further confirmed by confocal microscopy which, in addition, showed that **NP3** were actively internalized into the cytoplasm of the cells, especially the HEKß3 cells. Only a few HEKß1 cells were intensively labeled by **NP3**. Finally, both HEKß3 and HEKß1 cell lines were not labeled by **NP1**, suggesting that the peptide-decorated nanoparticles were more efficiently internalized inside the cells than the nanoparticles without peptide. This indicated that the affinity of cRGD clustered ligands for integrins favored a more pronounced cell internalization, possibly via active receptor-mediated pathways. The fact that this labeling was obtained in the presence of FCS suggested that **NP3** selectivity could be conserved *in vivo* as well as after administration in the blood stream.

In conclusion, the nanoparticles presenting cRGD-peptide tetravalent clusters in their outer corona demonstrated an enhanced internalization into cells over-expressing integrins. It confirmed that surface functionalization has a significant impact on the nanoparticle interaction with their surrounding biological environment. The possibility offered by the PISA-RAFT process to introduce group or ligand of interest precisely located at the chain-end of the soluble macroCTA "hairs" is thus a great advantage, notably to promote selective interactions with cell receptors and an active cell targeting.

Conclusions

We successfully developed a strategy to synthesize fluorescent and crosslinked PISA-RAFT nanoparticles decorated at their surface with a cRGD tetravalent peptide cluster located at the α-chain-end of the hydrophilic polymer block. A novel RAFT CTA functionalized with the cRGD tetravalent peptide cluster was synthesized and then used to control the NAM homopolymerization resulting in an original hydrophilic and biocompatible macroCTA presenting the peptide cluster at its α-chain-end (cRGDcluster-PNAM macroCTA). After optimization of the PISA-RAFT process to obtain 50-60 nm

spherical nanoparticles, we demonstrated that a crosslinker (to increase stability) and fluorescent monomers (for optical bioimaging) can be integrated to the nanoparticle hydrophobic core with no influence on polymerization kinetics nor on the final nanoparticle size. In addition, original peptide cluster-decorated nanoparticles were elaborated thanks to the cRGDcluster-PNAM macroCTA. Finally, both confocal microscopy and flow cytometry showed that the presence of the cRGD tetravalent peptide cluster at the surface of these PISA-RAFT nanoparticles enabled their selective internalization into live cells over-expressing integrins, that are the natural protein receptor of cRGD ligands.

Conflicts of interest

There are no conflicts to declare

Acknowledgements

We acknowledge Agnès Crépet (Laboratoire d'Ingénierie des Matériaux Polymères, Lyon) for technical support in SEC/MALLS, as well as Sandrine Denis-Quanquin (Laboratoire de Chimie, ENS de Lyon) for the DOSY NMR analyses. This work benefited from the facilities and expertise of the Liquid Chromatography and NMR Platforms of Institut de Chimie de Lyon, ICL (FR5223) for polymer characterization. Research at Institute for Advanced Biology (IAB, JLC and MH) was funded by the Institut National de la Santé et de la Recherche Médicale (INSERM, Paris France). We acknowledge the µcell imaging facility and in particular Dr Mylène Pezet. DB acknowledges the LabEx ARCANE and CBH-EUR-GS (ANR-17-EURE-0003), and the support from the ICMG Chemistry Nanobio Platform, Grenoble, for the peptide synthesis. We also thank Région Rhône-Alpes (ARC1 Santé) and La Ligue contre le Cancer, Comité du Rhône for financial support. The French/Portuguese binational collaborative work was also supported by Hubert Curien Partnership "PESSOA" program n°44648XM. D.D. acknowledges a PhD grant from the French Ministry of Research and Education.

Notes and references

1. E.-K. Lim, T. Kim, S. Paik, S. Haam, Y.-M. Huh and K. Lee, *Chemical Reviews*, 2015, **115**, 327-394.
2. Y. Zhong, F. Meng, C. Deng and Z. Zhong, *Biomacromolecules*, 2014, **15**, 1955-1969.
3. Z. Poon, S. Chen, A. C. Engler, H.-i. Lee, E. Atas, G. von Maltzahn, S. N. Bhatia and P. T. Hammond, *Angewandte Chemie International Edition*, 2010, **49**, 7266-7270.
4. C. J. Ferguson, R. J. Hughes, B. T. T. Pham, B. S. Hawkett, R. G. Gilbert, A. K. Serelis and C. H. Such, *Macromolecules*, 2002, **35**, 9243.
5. C. J. Ferguson, R. J. Hughes, D. Nguyen, B. T. T. Pham, R. G. Gilbert, A. K. Serelis, C. H. Such and B. S. Hawkett, *Macromolecules*, 2005, **38**, 2191.
6. M. Bathfield, F. D'Agosto, R. Spitz, M.-T. Charreyre, C. Pichot and T. Delair, *Macromolecular Rapid Communications*, 2007, **28**, 1540-1545.
7. N. J. Warren and S. P. Armes, *J. Am. Chem. Soc.*, 2014, **136**, 10174.
8. B. Charleux, G. Delaittre, J. Rieger and F. D'Agosto, *Macromolecules*, 2012, **45**, 6753-6765.
9. I. Chaduc, M. Girod, R. Antoine, B. Charleux, F. D'Agosto and M. Lansalot, *Macromolecules*, 2012, **45**, 5881-5893.
10. J. Wan, B. Fan and S. H. Thang, *Chemical Science*, 2022, **13**, 4192-4224.
11. V. J. Pansare, S. Hejazi, W. J. Faenza and R. K. Prud'homme, *Chemistry of Materials*, 2012, **24**, 812-827.
12. M. Monici, in *Biotechnology Annual Review*, Elsevier, 2005, vol. 11, pp. 227-256.
13. S. Adjili, A. Favier, G. Fargier, A. Thomas, J. Massin, K. Monier, C. Favard, C. Vanbelle, S. Bruneau, N. Peyriéras, C. Andraud, D. Muriaux and M.-T. Charreyre, *Biomaterials*, 2015, **46**, 70-81.
14. R. O. Hynes, *Nat Med*, 2002, **8**, 918-921.
15. M. Keramidas, V. Josserand, J.-J. Feige and J.-L. Coll, *Mol. Imaging Biol.*, 2013, **15**, 239-244.
16. H.-D. Kairbaan, *Current Opinion in Cell Biology*, 2008, **20**, 514-519.
17. M. Pfaff, K. Tangemann, B. Müller, M. Gurrath, G. Müller, H. Kessler, R. Timpl and J. Engel, *Journal of Biological Chemistry*, 1994, **269**, 20233-20238.
18. F. Danhier, A. L. Breton and V. Préat, *Molecular Pharmaceutics*, 2012, **9**, 2961-2973.
19. X. Chen, C. Plasencia, Y. Hou and N. Neamati, *Journal of Medicinal Chemistry*, 2005, **48**, 1098-1106.
20. D. Boturyn, J.-L. Coll, E. Garanger, M.-C. Favrot and P. Dumy, *Journal of the American Chemical Society*, 2004, **126**, 5730-5739.
21. D. Duret, A. Grassin, M. Henry, T. Jacquet, F. Thoreau, S. Denis-Quanquin, J.-L. Coll, D. Boturyn, A. Favier and M.-T. Charreyre, *Bioconjugate Chemistry*, 2017, **28**, 2241-2245.
22. A. Borbély, F. Thoreau, E. Figueras, M. Kadri, J.-L. Coll, D. Boturyn and N. Sewald, *Chemistry – A European Journal*, 2020, **26**, 2602-2605.
23. Z.-H. Jin, A. B. Tsuji, M. Degardin, A. Sugyo, S. Obara, H. Wakizaka, K. Nagatsu, K. Hu, M.-R. Zhang, P. Dumy, D. Boturyn and T. Higashi, *Clinical Cancer Research*, 2020, **26**, 6230-6241.
24. T. K. Mong, D. Charmot, J. M. Buysse, H. Chang, M. J. Cope and E. Goka, *Pharmaceutical compositions comprising a toxin-binding oligosaccharide and a polymeric particle*, Ilypsa Inc., Pat. WO2006044577 A1, 2006.
25. C. Ma, X. Liu, G. Wu, P. Zhou, Y. Zhou, L. Wang and X. Huang, *ACS Macro Letters*, 2017, **6**, 689-694.
26. L. Luppi, T. Babut, E. Petit, M. Rolland, D. Quemener, L. Soussan, M. A. Moradi and M. Semsarilar, *Polymer Chemistry*, 2019, **10**, 336-344.
27. T. Lückerath, K. Koynov, S. Loescher, C. J. Whitfield, L. Nuhn, A. Walther, C. Barner-Kowollik, D. Y. W. Ng and T. Weil, *Angewandte Chemie International Edition*, 2020, **59**, 15474-15479.
28. A. Favier, F. D'Agosto, M. T. Charreyre and C. Pichot, *Polymer*, 2004, **45**, 7821-7830.
29. A. Favier, M. T. Charreyre, P. Chaumont and C. Pichot, *Macromolecules*, 2002, **35**, 8271-8280.

30. M. Bathfield, F. D'Agosto, R. Spitz, M.-T. Charreyre and T. Delair, *Journal of the American Chemical Society*, 2006, **128**, 2546-2547.
31. S. Adjili, A. Favier, J. Massin, Y. Bretonniere, W. Lacour, Y.-C. Lin, E. Chatre, C. Place, C. Favard, D. Muriaux, C. Andraud and M.-T. Charreyre, *RSC Advances*, 2014, **4**, 15569-15578.
32. A. Favier, M. T. Charreyre and C. Pichot, *Polymer*, 2004, **45**, 8661-8674.
33. F. D'Agosto, M.-T. Charreyre, L. Veron, M.-F. Llauro and C. Pichot, *Macromolecular Chemistry and Physics*, 2001, **202**, 1689-1699.
34. M. Bencini, E. Ranucci, P. Ferruti, A. Manfredi, F. Trotta and R. Cavalli, *Journal of Polymer Science Part A: Polymer Chemistry*, 2008, **46**, 1607-1617.
35. E. Garanger, D. Boturyn, J.-L. Coll, M.-C. Favrot and P. Dumy, *Organic & Biomolecular Chemistry*, 2006, **4**, 1958-1965.
36. D. Boturyn, E. Defrancq, G. T. Dolphin, J. Garcia, P. Labbe, O. Renaudet and P. Dumy, *Journal of Peptide Science*, 2008, **14**, 224-240.
37. S. K. Misra, P. Kondaiah, S. Bhattacharya, D. Boturyn and P. Dumy, *Journal of Materials Chemistry B*, 2014, **2**, 5758-5767.
38. L. Sancey, E. Garanger, S. Foillard, G. Schoehn, A. Hurbin, C. Albiges-Rizo, D. Boturyn, C. Souchier, A. Grichine, P. Dumy and J.-L. Coll, *Mol Ther*, 2009, **17**, 837-843.
39. M. Degardin, D. Thakar, M. Claron, R. P. Richter, L. Coche-Guérente and D. Boturyn, *Journal of Materials Chemistry B*, 2017, **5**, 4745-4753.
40. S. Foillard, L. Sancey, J.-L. Coll, D. Boturyn and P. Dumy, *Organic & Biomolecular Chemistry*, 2009, **7**, 221-224.
41. A. Favier and M. T. Charreyre, *Macromolecular Rapid Communications*, 2006, **27**, 653-692.
42. C. Cepraga, A. Favier, F. Lerouge, P. Alcouffe, C. Chamignon, P.-H. Lanoe, C. Monnereau, S. Marotte, E. Ben Daoud, J. Marvel, Y. Leverrier, C. Andraud, S. Parola and M.-T. Charreyre, *Polymer Chemistry*, 2016, **7**, 6812-6825.
43. L. Bouvier-Fontes, R. Pirri, G. Arzamendi, J. M. Asua and J. R. Leiza, *Macromolecular Symposia*, 2004, **206**, 149-164.
44. F. Tronc, M. Li, J. Lu, M. A. Winnik, B. L. Kaul and J.-C. Graciet, *Journal of Polymer Science Part A: Polymer Chemistry*, 2003, **41**, 766-778.
45. K. Trofymchuk, J. Valanciunaite, B. Andreiuk, A. Reisch, M. Collot and A. S. Klymchenko, *Journal of Materials Chemistry B*, 2019, **7**, 5199-5210.
46. T. Ribeiro, S. Raja, A. S. Rodrigues, F. Fernandes, J. P. S. Farinha and C. Baleizão, *RSC Advances*, 2013, **3**, 9171-9174.
47. L. Sandrin, D. Thakar, C. Goyer, P. Labbe, D. Boturyn and L. Coche-Guerente, *Journal of Materials Chemistry B*, 2015, **3**, 5577-5587.